Optics Communications 342 (2015) 193–198

Contents lists available at ScienceDirect

Optics Communications

journal homepage: www.elsevier.com/locate/optcom

Far-field high resolution effects and manipulating of electromagnetic waves based on transformation optics

XueBin Ji, XiaoFei Zang*, Zhou Li, Cheng Shi, Lin Chen, Bin Cai, YiMing Zhu*

Shanghai Key Lab of Modern Optical System, Engineering Research Center of Optical Instrument and System, Ministry of Education, University of Shanghai for Science and Technology, Shanghai 200093, China

ARTICLE INFO

Article history:
Received 2 October 2014
Received in revised form
28 November 2014
Accepted 30 December 2014
Available online 31 December 2014

Keywords:
Transformation optics
Magnifying property
High-resolution
Far field

ABSTRACT

Based on the transformation optics (TO) and the effective medium theory (EMT), a new illusion media with homogeneous and isotropic materials is proposed to realize the far-field high resolution effects. When two point sources with the separation distance of $\lambda_0/4$ are covered with the illusion media (λ_0 is the free-space wavelength), the corresponding far-field pattern is equivalent to the case of two point sources with the separation distance larger than $\lambda_0/2$ in free space, leading to the far-field high resolution effects (in free space, the separation distance of $\lambda_0/4$ is less than half-wavelength, and thus the two point sources cannot be distinguished from each other). Furthermore, such illusion media can be applied to design tunable high-directivity antenna and an angle-dependent floating carpet cloak. Full wave simulations are carried out to verify the performance of our device.

1. Introduction

As a powerful tool, TO has attracted much attention for its major application in flexibly and accurately manipulating wave propagation paths in the past few years [1–3]. The main principle is based on the form invariance of Maxwell equations under coordinate transformation. By using a proper coordinate transformation, TO can be applied to design many fantastic devices, such as cloaks [4–21], field rotator [22,23], field concentrator [24], tunnel waves [25], antenna [26,27], retrodirective reflector [28], transparent wall [29], illusion systems [30–33], optical switch [34] and power combiner [35].

In this paper, TO is mainly applied into the field of high resolution effects. As is well known, the resolution of a conventional optical system is constrained to about half wavelength due to the loss of high spatial frequency information carried in the evanescent waves [36]. To break the diffraction limit, many approaches were adopted to realize high resolution effects. At first, the near-field scanning optical microscope was used to capture the evanescent waves from the near-field of the sample by a scanning probe [37–38]. However, it is inability to simultaneously observe different parts of the imaged objects and cannot produce a far-field direct imaging. Subsequently, superlens [39] with negative refraction index was proposed to allow the amplification of evanescent waves via the coupling between evanescent waves and surface plasmons. Although such superlens amplifies evanescent waves, it does not change the inherent exponential decaying character of evanescent waves in free space. In other words, both of them are confined to near-field high resolution and cannot produce a direct optical far-field imaging. In addition, hyperlens can convert evanescent waves to propagating waves by using anisotropic materials with hyperbolic dispersions [40–42], resulting in high resolution effects in the far-field region. And, until recently, hyperlens is the top choice to achieve high resolution. Here, we propose another way of illusion media to achieve high resolution effects in the far-field region. Different from hyperlens based on anisotropic materials, our design only demands layered homogeneous and isotropic materials, which is thus easier to realize. Furthermore, other applications of our device, such as tunable high-directivity antenna and an angle-dependent floating carpet cloak, are also investigated.

2. Theory

The geometric structure of the new illusion media is shown in Fig. 1(a). The whole transformation processes related to our designs are described as follows: The region of AFEDPQ and ABCDMN in virtual space are compressed into the region of ABCDPQ and AFEDMN in real space respectively. Meanwhile, in order to ensure the continuity of the whole transformed space, the transformational relationship in the hexagon region of ABCDEF (region VII) should be satisfied as $x' = x, y' = -y, z' = z$ (the index of transformation medium in this region is $n = -1$). The coordinate of each

* Corresponding authors.
E-mail addresses: xfzang@usst.edu.cn (X. Zang), ymzhu@usst.edu.cn (Y. Zhu).

http://dx.doi.org/10.1016/j.optcom.2014.12.078
0030-4018/

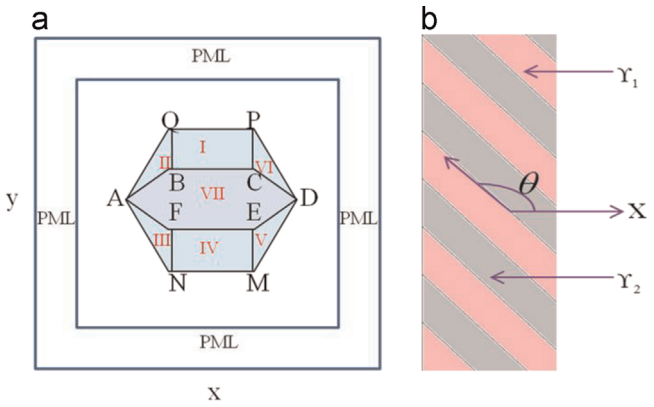

Fig. 1. (a) Schematic of the illusion media. (b) Schematic of layered structure with two kinds of isotropic materials to simplify the material parameters of the illusion media.

point is defined as follows: B $(-a_1, d/2)$, C $(a_1, d/2)$, E $(a_1, -d/2)$, F $(-a_1, -d/2)$, A $(-a_1-d, 0)$, D $(a_1+d, 0)$, Q $(-a_1, d)$, P (a_1, d), M $(a_1, -d)$, N $(-a_1, -d)$. The transformation equations between the real space and the virtual space can be expressed as:

Regions I and IV

$$x' = x,\ y' = \frac{1}{3}y \pm \frac{2}{3}d,\ z' = z \tag{1}$$

Regions II and V

$$x' = x,\ y' = \frac{2}{3}x + \frac{1}{3}y \pm \frac{2}{3}(a_1 + d),\ z' = z \tag{2}$$

Regions III and VI

$$x' = x,\ y' = -\frac{2}{3}x + \frac{1}{3}y \pm \frac{2}{3}(a_1 + d),\ z' = z \tag{3}$$

Region VII

$$x' = x,\ y' = -y,\ z' = z. \tag{4}$$

where "+" corresponds to regions I, II or VI and "−" corresponds to regions III, IV or V. According to the principle of the TO, the corresponding permittivity and permeability in region I–VII can be calculated by using $Y' = \Lambda Y \Lambda^T / det(\Lambda)$.

Regions I and IV

$$\varepsilon_r' = \mu_r' = \begin{pmatrix} 3 & 0 & 0 \\ 0 & \frac{1}{3} & 0 \\ 0 & 0 & 3 \end{pmatrix} \tag{5}$$

Regions II and V

$$\varepsilon_r' = \mu_r' = \begin{pmatrix} 3 & 2 & 0 \\ 2 & \frac{5}{3} & 0 \\ 0 & 0 & 3 \end{pmatrix} \tag{6}$$

Regions III and VI

$$\varepsilon_r' = \mu_r' = \begin{pmatrix} 3 & -2 & 0 \\ -2 & \frac{5}{3} & 0 \\ 0 & 0 & 3 \end{pmatrix} \tag{7}$$

Region VII

$$\varepsilon_r' = \mu_r' = \begin{pmatrix} -1 & 0 & 0 \\ 0 & -1 & 0 \\ 0 & 0 & -1 \end{pmatrix} \tag{8}$$

From Eqs. (6) and (7), the constitutive electromagnetic parameters are spatially invariant. According to EMT, such homogeneous but anisotropic materials can be replaced by using an alternating layered medium with homogeneous and isotropic materials. Based on EMT, a real symmetric tensor can be mapped into diagonal tensor by rotating a certain angle θ as follows:

$$Y = \begin{pmatrix} Y_{xx} & Y_{xy} & 0 \\ Y_{xy} & Y_{yy} & 0 \\ 0 & 0 & Y_{zz} \end{pmatrix} = \begin{pmatrix} \cos\theta & -\sin\theta & 0 \\ \sin\theta & \cos\theta & 0 \\ 0 & 0 & 1 \end{pmatrix} \begin{pmatrix} Y_x^C & 0 & 0 \\ 0 & Y_y^C & 0 \\ 0 & 0 & Y_{zz} \end{pmatrix} \begin{pmatrix} \cos\theta & \sin\theta & 0 \\ -\sin\theta & \cos\theta & 0 \\ 0 & 0 & 1 \end{pmatrix} \tag{9}$$

$$Y_{x,y}^C = \left[Y_{xx} + Y_{yy} \pm \sqrt{(Y_{xx} - Y_{yy})^2 + (2Y_{xy})^2} \right] / 2 \tag{10}$$

The angle θ can be obtained by using the following formula:

$$\tan(2\theta) = \frac{2Y_{xy}}{Y_{xx} - Y_{yy}} \tag{11}$$

According to the EMT, if the layers are parallel to the local x–z plane and the thickness of each medium layer is much less than the wavelength, Eq. (10) can be simplified written as

$$Y_x^C = Y_z^C = \frac{\Upsilon_1 + \eta\Upsilon_2}{1 + \eta}, \tag{12a}$$

$$Y_y^C = \frac{(1 + \eta)\Upsilon_1\Upsilon_2}{\eta\Upsilon_1 + \Upsilon_2}, \tag{12b}$$

where Υ_1, Υ_2 are the parameters of two isotropic mediums, η is the ratio of thicknesses between these two alternating layered mediums. For the transverse electric (TE) wave, $\Upsilon_1 = \mu_i^A$ and $\Upsilon_2 = \mu_i^B$, where μ_i^A and μ_i^B correspond to the permeability parameters of the layered isotropic medium-A and medium-B, respectively (i=I–VI). Thus, in the case of η=1, the layered homogeneous and isotropic parameters required in regions I–VI are $\mu_j^A = 5.8284$, $\mu_j^B = 0.1716$, $\varepsilon_j = 3$ (j=I and IV) and $\mu_k^A = 8.769$, $\mu_k^B = 0.114$, $\varepsilon_k = 3$ (k=II, III, V and VI).

3. Numerical simulation and discussion

First, we investigate far-field high resolution effects by virtue of the illusion media. In region I and IV, the region QPCB in real space is mapped into the region QPEF in virtual space, a small longitudinal distance (d) in the region QPCB would be equivalent to a larger longitudinal distance (D) in virtual space, with D=3d. Thus, the wavelength in region I and IV is satisfied as $\lambda_0 = 3\bar{\lambda}$ (in y-direction), where λ_0 and $\bar{\lambda}$ are the free-space wavelength and in-material wavelength, respectively. If two point sources with separation distance $\lambda_0/4$ in free space, they cannot be distinguished due to the diffraction limit. But, when these two point sources are embedded in the transformation region I and IV, the separation distance is still $\lambda_0/4$ (and $\lambda_0/4 = 3\bar{\lambda}/4$), but they can be easily distinguished. Here, we want to emphasize that although $\lambda_0/4 = 3\bar{\lambda}/4$ in physical space, the distance between these two point sources in transformation region I and IV is enlarged effectively to that of $3\lambda_0/4$ in the virtual space, as described in Ref [43]. When two point sources O_1, O_2 are located at (0, 0.315 mm) and (0, 0.269 mm),

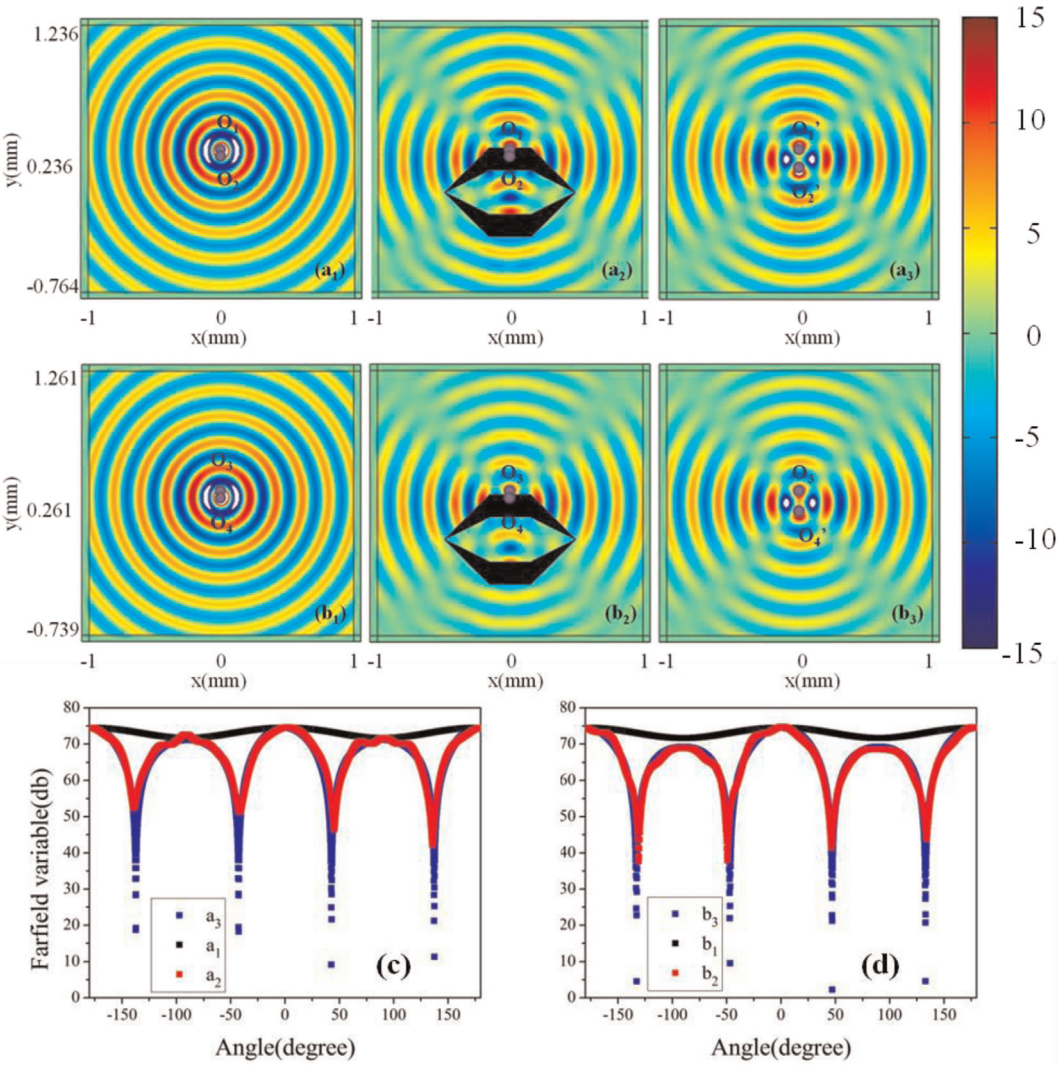

Fig. 2. The field distribution of two sources (O_1 and O_2) (a_1) or (O_3 and O_4) (b_1) in free space. The field distribution of two sources (O_1 and O_2) (a_2) or (O_3 and O_4) (b_2) covered with the illusion media. The field distribution of two sources (O_1' and O_2') (a_3) or (O_3 and O_4') (b_3) in free space. (c) The corresponding far-field patterns at $r=1.875$ mm ($10\lambda_0$) of (a_1) (black line), (a_2) (red line) and (a_3) (blue line). (d) The corresponding far-field patterns at $r=1.875$ ($10\lambda_0$) mm of (b_1) (black line), (b_2) (red line) and (b_3) (blue line). (For interpretation of the references to color in this figure legend, the reader is referred to the web version of this article.)

respectively, with frequency of 1.6 THz, the separation distance between these two point sources is about $\lambda_0/4$ (0.046 mm), thus the two sources cannot be distinguished from each other in free space (Fig. 2(a_1)). When the two sources (O_1 and O_2) are embedded in the region QPCB (Fig. 2(a_2)), both of them are mapped into O_1' (0, 0.305 mm) and O_2' (0, 0.167 mm), respectively, in virtual space. Fig. 2(a_3) depicts the field distribution of two sources located at O_1' and O_2', respectively, in free space. The distance between these two sources (O_1' and O_2') is about 0.74 λ_0 (0.138 mm), and thus the two sources can be easily separated in free space based on the diffraction limit theory. Both the field distributions in Fig. 2(a_2) and (a_3) have the same features. That is to say, based on the illusion media, the field distribution of two point sources (O_1 and O_2) with the separation distance of $\lambda_0/4$ (or $3\bar{\lambda}/4$ in transformation medium) in Fig. 2(a_2) is equivalent to the case of two point sources (O_1' and O_2') with the separation distance of $0.74\lambda_0$ in Fig. 2(a_3) in free space, resulting in high resolution effects (as described in Ref [43]). Now, we perform a further study of high resolution effects with only one of the two point sources in physical space embedding into the region QPCB. Two point sources O_3, O_4 are located at (0, 0.325 mm) and (0, 0.279 mm), respectively, as shown in Fig. 2(b_1). They still cannot be distinguished from each other in free space. When the point source O_4 embedded in the region QPCB as shown in Fig. 2(b_2), it is mapped into O_4' (0, 0.197 mm) in virtual space. Fig. 2(b_3) depicts the field distribution of two sources located at O_3 and O_4', respectively, in free space. The distance between these two sources (O_3 and O_4') is about $0.68\lambda_0$ (0.128 mm), and the two sources can be distinguished in free space. The field distributions in Fig. 2(b_2) and (b_3) are nearly the same, which means that based on the illusion media, the field distribution of the two sources (O_3 and O_4) with the separation distance of $\lambda_0/4$ in Fig. 2(b_2) is also equivalent to the case of two sources (O_3 and O_4') with the separation distance of $0.68\lambda_0$ in Fig. 2(b_3) in free space, leading to high resolution effects. In order to demonstrate the high resolution effects in the far-field region, we show the corresponding far-field patterns in Figs. 2(c) and (d). Obviously, the two point sources without coating with the transformation medium are almost overlapped with each other with nearly homogeneous field intensity along a straight line with radius $r=1.875$ mm ($r=10\lambda_0$) and thus cannot be distinguished in free space (see black lines in Figs. 2(c) and (d)) as discussed in Ref [43]. However, when the two point sources are covering with the illusion media (see red lines in Fig. 2(c) and (d)), the corresponding far-field pattern shows a series of dips and peaks, and it is nearly equivalent to the case of two point sources with separation distance of $0.74\lambda_0$ (or $0.68\lambda_0$) in free space (see

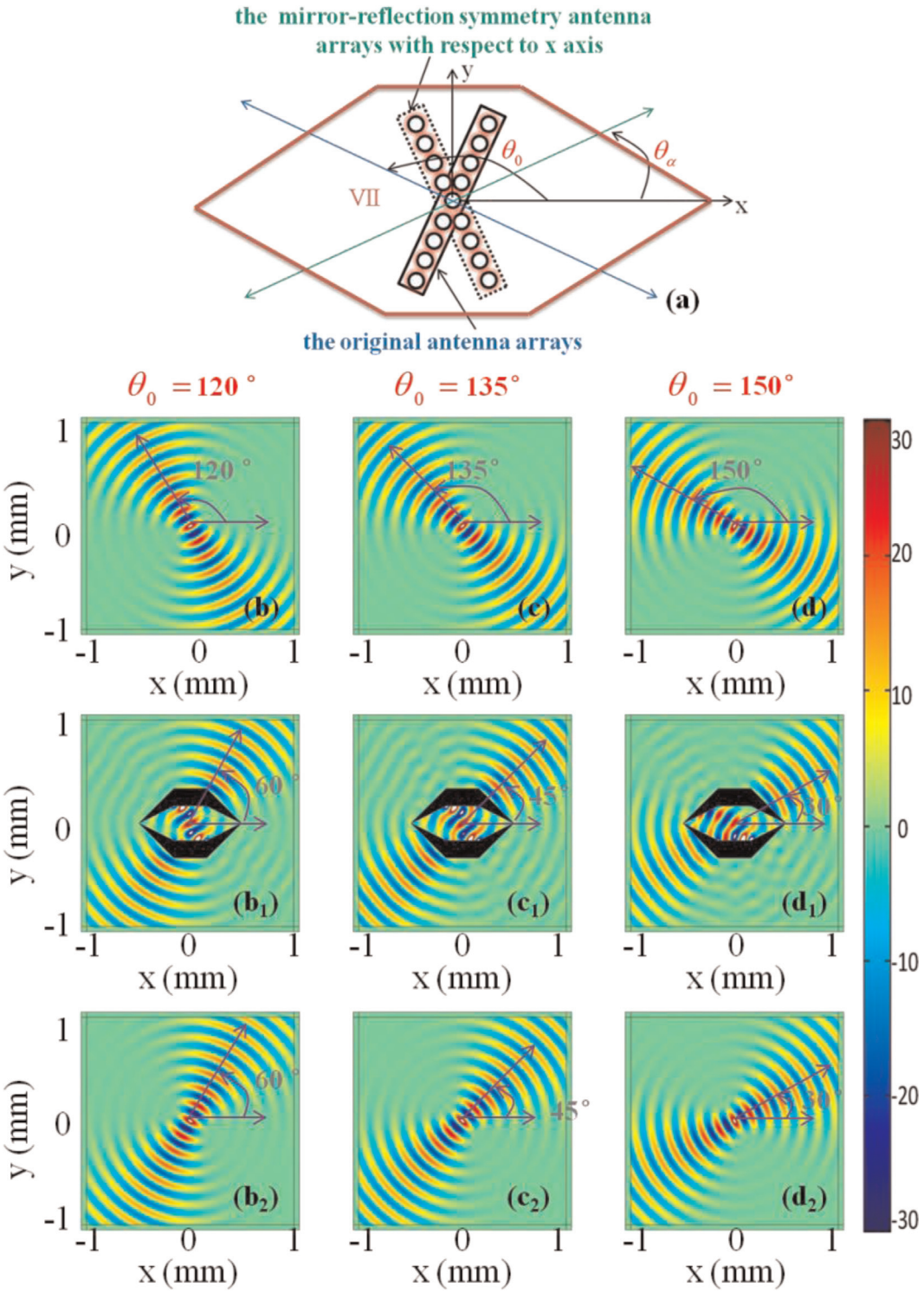

Fig. 3. (a) The schematic of the transformation of the antenna arrays inside the region VII (the blue line stands for the radiation direction of the original antenna arrays while the green line stands for the radiation direction of the mirror-reflection symmetry antenna arrays). The field distribution of the antenna array in free space when the radiating direction of the antenna arrays are 120° (b), 135° (c) or 150° (d), respectively. The field distribution of the antenna array covered with the illusion media when the radiating directions of the antenna arrays are 120° (b_1), 135° (c_1) or 150° (d_1), respectively. The field distribution of the antenna array in free space when the radiating directions of the antenna arrays are 60° (b_2), 45° (c_2) or 30° (d_2), respectively. (For interpretation of the references to color in this figure legend, the reader is referred to the web version of this article.)

blue lines in Fig. 2(c) and (d)). Meanwhile, the four peaks and the four dips in the far-field patterns are induced by the coherent effect of the two distinguished point sources (O_1' and O_2'; O_3 and O_4'), demonstrating far-field high resolution effects. Therefore, we can achieve far-field high resolution effects by using the illusion media.

Next, we investigate tunable high-directivity antennas by using this illusion media. Here, a nine-element point sources array is designed to simulate the high-directivity antennas (the proportion of the current distribution on each point source is 1/70:4/35:2/5:4/5:1:4/5:2/5:4/35:1/70 with the operating frequency of each point source is 2 THz), and the radiation angle of the antenna arrays in free space is θ_0, as shown in Fig. 3. In this case, the antenna arrays

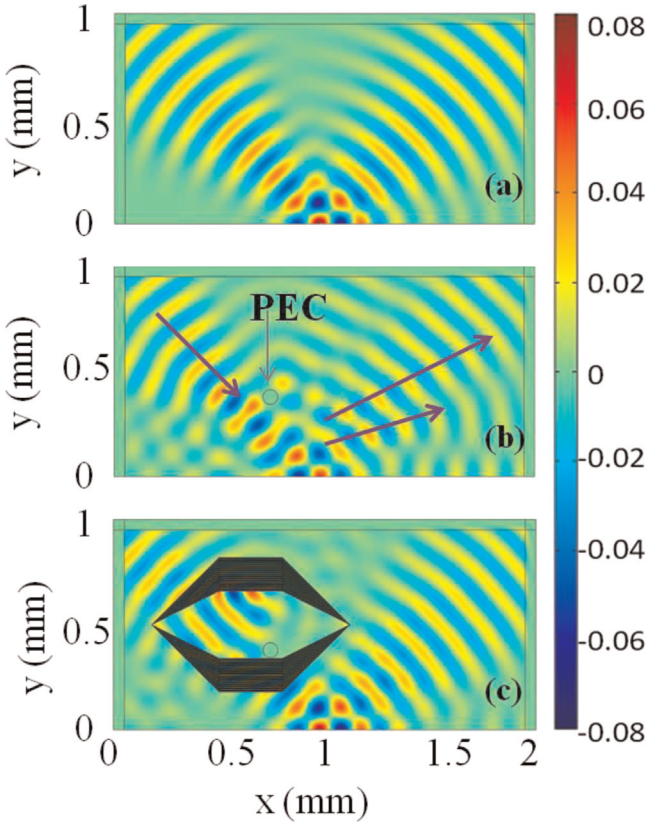

Fig. 4. (a) The field distribution when a Gaussian beam is launched at 45° toward the ground; (b) The field distribution when a circular-shaped PEC is placed above the ground plane; (c) The field distribution when the same circular-shaped PEC is covered with the illusion media.

are embedded into the region VII. According to the transformation relationship in region VII ($x' = x, y' = -y, z' = z$), each point source is mapped to its mirror-reflection symmetry point with respect to x axis. So, when the antenna arrays are embedded into the region VII, the corresponding radiation angle θ_α outside the illusion media can be described by $\theta_\alpha = 180 - \theta_0$, as shown in Fig. 3 (a). Fig. 3(b–d) shows the field distribution of the antenna arrays in free space when the radiating directions of the antenna arrays are 120°, 135° and 150°, respectively. When they are covered with the illusion media, the radiating directions of the antenna arrays outside the illusion media are 60° (Fig. 3(b_1)), 45° (Fig. 3(c_1)) and 30° (Fig. 3(d_1)), respectively. Fig. 3(b_2), (c_2), and (d_2) shows the field distribution of the antenna arrays in free space when the radiating directions of the antenna arrays are 60°, 45° and 30°, respectively. The field distributions in Fig. 3(b_2), (c_2) and (d_2) are nearly the same as those in Fig. 3(b_1), (c_1) and (d_1), respectively, demonstrating the tunable effect of the illusion media. Therefore, we can flexibly control the radiation direction of the antenna arrays by rotating the transformation medium.

Finally, we study an angle-dependent floating carpet cloak based on such illusion media. Fig. 4(a) shows the field distribution when a 2 THz Gaussian beam transmits to a PEC ground plane with incident angle of 135°. When a circular-shaped PEC is embedded into the propagating path of the incident electromagnetic wave, significant scattered field is induced by the PEC as shown in Fig. 4(b). When the same PEC is covered with the illusion media (Fig. 4(c)), the incident Gaussian beam is rotated 90° clockwise inside transformation region VII and then irradiates straight on the ground plane without interacting with the circular-shaped PEC. The field distribution in Fig. 4(c) is nearly the same as that in Fig. 4 (a), verifying the cloaking property of the illusion media. Here, it should be noted that the PEC is placed above the ground plane rather than closed to the ground plane and the illusion media is only valid for detecting waves of specific incident angles. So, the illusion media can be considered as an angle-dependent floating carpet cloak, which successfully protects the PEC flying over the ground plane from detecting waves of specific incident directions.

4. Conclusion

In summary, we have theoretically proposed a new illusion media by using homogeneous and isotropic materials to realize far field high resolution effects. In addition, tunable high-directivity antenna and an angle-dependent floating carpet cloak based on such illusion media are also investigated. Both the theory model and numerical simulations prove that the new illusion media has many potential applications in the field of transformation optical devices.

Acknowledgments

This work is partly supported by the National Program o Key Basic Research Project of China (973 Program, 2014CB339806), Major National Development Project of Scientific Instrument and Equipment (2011YQ150021, 2012YQ14000504, 2012YQ150092), National Natural Science Foundation of China (61138001, 61205094, 61307126), the Key Scientific and Technological Project of Science and Technology Commission of Shanghai Municipality (2014XD140300) (12JC1407100), the Scientific Research Innovation Project of Shanghai Municipal Education Commission (14YZ093), and New Century Excellent Talents from Ministry of Education (NCET-12-1052) and the university young teacher training scheme of Shanghai (ZZSLG13015).

References

[1] J.B. Pendry, D. Schurig, D.R. Smith, Controlling electromagnetic fields, Science 312 (2006) 1780.
[2] U. Leonhardt, Optical conformal mapping, Science 312 (2006) 1777.
[3] H.Y. Chen, C.T. Chan, P. Sheng, Transformation optics and metamaterials, Nat. Mater. 9 (2010) 387.
[4] D. Schurig, J.J. Mock, B.J. Justice, S.A. Cummer, Metamaterial electromagnetic cloak at microwave frequencies, Science 314 (2006) 977.
[5] M. Rahm, D. Schurig, D.A. Roberts, Design of electromagnetic cloaks and concentrators using form-invariant coordinate transformations of Maxwell's equations, Photon. Nanostruct. Fundam. Appl 6 (2008) 87.
[6] W.X. Jiang, T.J. Cui, G.X. Yu, X.Q. Lin, Arbitrarily elliptical-cylindrical invisible cloaking,, J. Phys. D 41 (2008) 085504.
[7] H. Ma, S. Qu, Z. Xu, J. Wang, The open cloak, Appl. Phys. Lett. 94 (2009) 103501.
[8] T.C. Han, C.W. Qiu, X.H. Tang, The general two-dimensional open-closed cloak with tunable inherent discontinuity and directional communication, Appl. Phys. Lett. 97 (2010) 124104.
[9] J. Li, J.B. Pendry, Hiding under the carpet: a new strategy for cloaking, Phys. Rev. Lett. 101 (2008) 203901.
[10] R. Liu, J.J. Mock, C. Ji, Broadband ground-plane cloak, Science 323 (2009) 366.
[11] J. Valentine, J. Li, T. Zentgraf, G. Bartal, An optical cloak made of dielectrics, Nat. Mater. 8 (2009) 568.
[12] Y. Luo, J.J. Zhang, H.S. Chen, A rigorous analysis of plane-transformed invisibility cloaks, IEEE 57 (2009) 3926.
[13] S. Xi, H.S. Chen, B.I. Wu, One-directional perfect cloak created with homogeneous material, IEEE 19 (2009) 131.
[14] J.J. Zhang, L. Liu, Y. Luo, Homogeneous optical cloak constructed with uniform layered structures, Opt. Express 19 (2011) 8625.
[15] X.F. Xu, Y.J. Feng, Y. Hao, Infrared carpet cloak designed with uniform silicon grating structure, Appl. Phys. Lett. 95 (2009) 184102.
[16] L. Lan, F. Sun, Y.C. Liu, C.K. Ong, Experimentally demonstrated a unidirectional electromagnetic cloak designed by topology optimization, Appl. Phys. Lett. 103 (2013) 12113.
[17] G. Fujii, H. Watanabe, T. Yamada, Level set based topology optimization for optical cloaks,, Appl. Phys. Lett. 102 (2013) 251106.
[18] Y. Lai, H.Y. Chen, Z.Q. Zhang, C.T. Chan, Complementary media invisibility cloak that cloaks objects at a distance outside the cloaking shell, Phys. Rev. Lett. 102

(2013) 093901.
[19] T.Y. Huang, H.C. Lee, L.W. Un, An innovative cloak enables arbitrary multi-objects hidden with visions and movements, Appl. Phys. Lett. 101 (2012) 151901.
[20] W.R. Zhu, C.L. Ding, X.P. Zhao, Numerical method for designing acoustic cloak with homogeneous metamaterials, Appl. Phys. Lett. 97 (2010) 131902.
[21] W.R. Zhu, I. Shadrivov, D. Powell, Y. Kivshar, Hiding in the corner,, Opt. Express 19 (2011) 20827.
[22] H.Y. Chen, C.T. Chan, Transformation media that rotate electromagnetic fields, Appl. Phys. Lett. 90 (2007) 241105.
[23] X.F. Zang, Z. Li, C. Shi, L. Chen, Rotatable illusion media for manipulating terahertz electromagnetic waves, Opt. Express 21 (2013) 25565.
[24] W.X. Jiang, T.J. Cui, Q. Cheng, Design of arbitrarily shaped concentrators based on conformally optical transformation of nonuniform rational B-spline surfaces, Appl. Phys. Lett. 92 (2008) 264101.
[25] T.C. Han, C.W. Qiu, X.H. Tang, Homogeneous and isotropic bends to tunnel waves through multiple different/equal waveguides along arbitrary directions, Opt. Express 19 (2011) 13020.
[26] L.J. Huang, X.S. Chen, B. Ni, Design of highly directive antenna made of homogeneous media, J. Opt. Soc. Am. B 29 (2012) 113150.
[27] W.X. Jiang, T.J. Cui, H.F. Ma, X.M. Yang, Q. Cheng, Layered high-gain lens antennas via discrete optical transformation, Appl. Phys. Lett. 93 (2008) 221906.
[28] S. Xiong, Y.J. Feng, T. Jiang, Designing retrodirective reflector on a planar surface by transformation optics,, AIP Adv. 3 (2013) 012113.
[29] Z.L. Mei, Y.L. Xu, J. Bai, T.J. Cui, Nonmagnetic electromagnetic transparent wall realized by a metal-dielectric multilayer structure, Opt. Express 20 (2012) 16955.
[30] Y. Lai, J. Ng, H.Y. Chen, D.Z. Han, J.J. Xiao, Illusion optics: the optical transformation of an object into another object, Phys. Rev. Lett. 102 (2009) 253902.
[31] X.F. Zang, B. Cai, Y.M. Zhu, Shifting media for carpet cloaks, antiobject independent illusion optics, and a restoring device, Appl. Opt. 52 (2013) 1832.
[32] Y. Shen, K. Ding, W.J. Sun, L. Zhou, A chirality switching device designed with transformation optics, Opt. Express 18 (2010) 21419.
[33] T. Yang, H.Y. Chen, X.D. Luo, H.R. Ma, Superscatterer: enhancement of scattering with complementary media, Opt. Express 16 (2008) 18545.
[34] H.R. Shoorian, M.S. Abrishamian, Design of optical switches by illusion optics, J. Opt. 15 (2013) 055107.
[35] Y. Luo, S.Z. Zhu, A power combiner and multisource co-beam reflector based on virtual shifting of the sources using negative index media, J. Opt. 14 (2012) 105102.
[36] M. Born, E. Wolf, Principles of Optics, Cambridge University Press, Cambridge, 1999.
[37] D.W. Pohl, W. Denk, M. Lanz, Optical stethoscopy: image recording with resolution λ/20, Appl. Phys. Lett. 44 (1984) 651.
[38] Lewis, M. Isaacson, A. Harootunian, A. Muray, "Development of a 50 nm spatial resolution light microscope,", Ultramicroscopy 13 (1984) 227–231.
[39] N. Fang, H. Lee, C. Sun, X. Zhang, Sub-diffraction-limited optical imaging with a silver superlens, Science 308 (2005) 534.
[40] Z. Jacob, L.V. Alekseyev, E. Narimanov, Optical hyperlens: far-field imaging beyond the diffraction limit, Opt. Express 14 (2006) 8247.
[41] J. Rho, Z.L. Ye, Y. Xiong, X.B. Yin, Spherical hyperlens for two-dimensional sub-diffractional imaging at visible frequencies, Nat. Commun. 1148 (2010).
[42] Z. Liu, H. Lee, Y. Xiong, C. Sun, Far-field optical hyperlens magnifying sub-diffraction-limited objects, Science 315 (2007) 1686.
[43] W.X. Jiang, C.W. Qiu, T.C. Han, Q. Cheng, H.F. Ma, S. Zhang, T.J. Cui, Broadband all-dielectric magnifying lens for far-field high-resolution imaging,, Adv. Mater. 25 (2013) 6963.